Journal of Materials and Electronic Devices 1 (2025) 29-36

Synthesis, Characterization, and Investigation of Optical Properties of New Schiff Base-Boron Complexes Bearing Sulfonamide Moiety

Melek TERCAN[a], Diğdem ERDENER[a], Namık ÖZDEMİR[b], Osman DAYAN[a]

[a] Department of Chemistry, Faculty of Arts and Sciences, Çanakkale Onsekiz Mart University, Çanakkale, Türkiye
[b] Department of Physics, Faculty of Science, Ondokuz Mayıs University, 55139 Samsun, Türkiye

This article presents the synthesis of a series of new boron complexes containing a sulfonamide moiety and the characterization of their structures using spectroscopic methods, including FT-IR, UV-Vis, ^{1}H-NMR, ^{13}C-NMR, and ESI-MS. Theoretical and experimental investigations of the optical properties of the synthesized compounds also revealed their optical band gaps and maximum absorption wavelengths. The theoretical calculations were carried out using the Gaussian09 package at the HSEH1PBE/cc-pVDZ level of theory, and the molecular frontier orbitals (HOMO-LUMO) were analyzed. Comparative evaluation of the experimental and theoretical data showed that the newly synthesized sulfonamide-derived boron complexes exhibited distinct fluorescence properties.

Keywords: *N,O-donor ligands, Boron complexes, Sulfonamides, optical properties, DFT*

Submission Date: 19 June 2025
Acceptance Date: 29 August 2025

**Corresponding author: osmandayan@comu.edu.tr (Osman DAYAN)*

1. Introduction

Boron complexes are commonly utilized in solar energy conversion systems, optical sensors, and hydrogen production/storage applications due to their optical and electrical features [1]. The use of boron compounds as dyes is very common. BODIPY, or 4,4-difluoro-4-bora-3a,4a-diaza-s-indacene, is the most well-known chemical in this class [2-8].

Boron rapidly forms complexes with Schiff bases, including N and O donors capable of producing chelate rings. Combining Schiff bases from 2-hydroxyamine derivatives with $BF_3.OEt_2$ is a simple way to synthesize these complexes. According to the literature, these types of complexes have outstanding optical properties and are useful in dye manufacturing, optoelectric materials, and medicinal chemistry [9-16].

Schiff bases are highly preferred ligands due to their ease of synthesis and ability to control the charge density and stericity of the complex by selecting appropriate R groups. Schiff base complexes are employed in a variety of applications, including sensors, catalysis, polymer technology, the pharmaceutical industry, medicinal chemistry, agriculture, and biological systems, and extensive research into new syntheses is ongoing. Schiff base derivatives are also widely employed in the manufacturing of optoelectronic materials [17-19]. Because of their capacity to produce chelates, 2-hydroxy Schiff bases are receiving more attention in the literature [20, 21].

In this paper, six Schiff base ligands with N,O donors and six Schiff base-boron complexes were synthesized from their reaction with $BF_3.OEt_2$, and their structures were studied using FT-IR, UV-vis, ^{1}H-NMR, ^{13}C-NMR, and ESI-MS techniques. The optical properties of synthesized compounds were examined.

2. Methods and Materials

Experimental

All reactions were carried out under an argon atmosphere using the Schlenk technique. Chemicals were purchased from commercial suppliers and used without further purification. NMR spectra were recorded at 297 K on a Jeol JNM-ECX400II instrument. IR spectra were obtained with a Perkin Elmer Spectrum One FTIR instrument equipped with

an ATR sampling accessory. UV-Vis spectra were recorded using a Thermo Scientific Evolution 201 instrument. Mass spectra were acquired on a Shimadzu LC-MSMS-8040 instrument. **La-c** compounds were synthesized according to literature procedures [22-25].

Synthesis of L1a-c

L1a [22] and **L1c** [26] were synthesized following methods described in the literature. **L1b** (5 mmol) and salicylaldehyde (5 mmol) were stirred in methanol (25 mL) at room temperature for 24 hours. After this period, the solution was concentrated and allowed to crystallize. The resulting crystals (**L1a-c**) were filtered and air-dried.

*Data for **L1b***

^{1}H NMR (400 MHz, $CDCl_3$) δ ppm 2.24 (s, 3 H) 2.30 (s, 3 H) 6.64 - 6.76 (m, 2 H) 6.94 (t, J=8.01 Hz, 1 H) 7.01 (d, J=8.24 Hz, 1 H) 7.17 - 7.28 (m, 3 H) 7.33 - 7.44 (m, 2 H) 7.47 (s, 1 H) 7.65 (d, J=7.33 Hz, 2 H) 8.05 (s, 1 H) 11.89 (s, 1 H) ^{13}C NMR (101 MHz, $CDCl_3$) δ ppm 19.42 19.55 117.18 118.89 119.30 119.63 126.01 126.97 127.16 128.72 132.52 132.68 133.64 135.73 136.57 138.97 139.84 160.35 163.96. FT-IR (cm^{-1}) 685, 721, 754, 771, 799, 842, 863, 899, 916, 970, 1008, 1026, 1085, 1121, 1157, 1292, 1328, 1372, 1383, 1412, 1446, 1493, 1566, 1604, 1617, 2920, 2944, 2970, 3060, 3354.

*Data for **L1c***

^{1}H NMR (400 MHz, $CDCl_3$) δ ppm 6.48 (s, 1 H) 6.80 (s, 1 H) 6.83 - 6.91 (m, 1 H) 6.98 (d, *J*=8.43 Hz, 1 H) 7.19 (s, 1 H) 7.33 (t, *J*=6.32 Hz, 2 H) 7.51 (t, *J*=8.08 Hz, 2 H) 7.65 (t, *J*=7.38 Hz, 1 H) 7.91 (d, *J*=7.03 Hz, 2 H) 8.54 (s, 1 H) 12.56 (s, 1 H). ^{13}C NMR (101 MHz, $CDCl_3$) δ ppm 117.64 117.80 118.43 118.84 119.27 121.14 128.90 129.12 130.94 132.67 133.42 134.06 134.52 135.27 138.59 141.97 146.35 161.32 164.63. FT-IR (cm^{-1}) 682, 703, 722, 739, 755, 842, 864, 880, 912, 1000, 1084, 1130, 1163, 1252, 1278, 1314, 1353, 1377, 1449, 1470, 1480, 1583, 1620, 2922, 3072, 3101, 3377, 3409, 3473, 3500.

Synthesis of L2a-c

L2a [27] was synthesized following methods described in the literature. **La-c** (5 mmol) and 2-hydroxy-1-naftaldehyde (5 mmol) were stirred in methanol (25 mL) at room temperature for 24 hours. After this period, the solution was concentrated and left to crystallize. The resulting crystals (**L2a-c**) were filtered and air-dried.

*Data for **L2a***

^{1}H-NMR (400 MHz, $CDCl_3$) δ ppm 7.01 (d, *J*=7.8 Hz, 1 H), 7.16 - 7.26 (m, 4 H), 7.33 (t, *J*=7.6 Hz, 1 H), 7.42 (t, *J*=7.6 Hz, 1 H), 7.57 (t, *J*=7.6 Hz, 1 H), 7.68 (d, *J*=7.4 Hz, 2 H), 7.73 (d, *J*=7.8 Hz, 1 H), 7.82 (d, *J*=7.8 Hz, 1 H), 7.92 (d, *J*=9.2 Hz, 1 H), 7.97 (d, *J*=8.8 Hz, 1 H), 8.93 (s, 1 H). ^{13}C NMR (101 MHz, $CDCl_3$) δ ppm 109.6, 119.4, 119.5, 119.7, 124.0, 124.5, 127.1, 127.2, 127.7, 127.9, 128.3, 128.9, 129.5, 129.8, 132.6, 132.9, 136.3, 138.8, 142.2, 161.0, 163.3. FT-IR (cm^{-1}) 685, 722, 734, 749, 837, 866, 909, 946, 971, 1042, 1091, 1141, 1163, 1213, 1288, 1320, 1360, 1394, 1452, 1491, 1531, 1545, 1592, 1618, 3070, 3246, 3579.

*Data for **L2b***

^{1}H NMR (400 MHz, $CDCl_3$) δ ppm 2.28 (s, 3 H) 2.32 (s, 3 H) 6.78 (s, 2 H) 7.09 - 7.22 (m, 4 H) 7.41 (t, *J*=7.10 Hz, 1 H) 7.49 (s, 1 H) 7.56 (t, *J*=7.10 Hz, 1 H) 7.61 - 7.67 (m, 2 H) 7.81 (d, *J*=7.79 Hz, 1 H) 7.89 (d, *J*=8.70 Hz, 1 H) 7.96 (d, *J*=8.70 Hz, 1 H) 8.84 (s, 1 H). ^{13}C NMR (101 MHz, $CDCl_3$) δ ppm 19.5, 19.6, 109.5, 119.3, 119.8, 120.1, 123.8, 126.6, 126.9, 127.0, 127.8, 128.0, 128.7, 129.4, 132.5, 135.8, 136.1, 136.4, 138.8, 140.0, 159.4, 164.0. FT-IR (cm^{-1}) 684, 714, 725, 752, 780, 835, 869, 900, 925, 971, 999, 1017, 1040, 1086, 1139, 1156, 1193, 1210, 1254, 1301, 1352, 1411, 1446, 1488, 1522, 1542, 1602, 1617, 2969, 3052, 3090.

*Data for **L2c***

^{1}H NMR (400 MHz, $CDCl_3$) δ ppm 6.56 (s, 1 H) 6.87 (s, 1 H) 7.55 - 7.66 (m, 5 H) 7.71 – 7.78 (m, 2 H) 7.96 – 8.02 (m, 5 H) 10.84 (s, 1 H). ^{13}C NMR (101 MHz, $CDCl_3$) δ ppm 117.8 118.5 118.6 119.2 120.5 120.7 123.91 124.5 128.3 128.9 129.1 130.0 133.5 135.0 135.6 136.9 138.7 139.2 146.4 157.8 165.0. FT-IR (cm^{-1}) 684, 701, 724, 737, 758, 795, 815, 841, 863, 880, 912, 968, 1000, 1036, 1084, 1128, 1143, 1162, 1175, 1214, 1245, 1273, 1313, 1347, 1377, 1395, 1450, 1463, 1480, 1557, 1588, 1620, 2921, 3074, 3099, 3410, 3501.

General Method for the Synthesis of 1 – 6

L(1-2)(a-c) (1 mmol) and triethylamine (10 mmol) were stirred in toluene for 1 hour at room temperature under an argon atmosphere. After stirring, $BF_3.OEt_2$ (10 mmol) was added to the mixture, and stirring continued at 80 °C for 1 day. Upon completion of the reaction, the solution was concentrated to dryness and washed with water. The product was then crystallized from methanol.

*Data for **1***

^{1}H NMR (400 MHz, $CDCl_3$) δ ppm 6.39 (s, 1 H) 6.73 (d, *J*=7.42 Hz, 1 H) 6.89 - 7.00 (m, 1 H) 7.04 (d, *J*=8.20 Hz, 1 H) 7.10 - 7.34 (m, 4 H) 7.39 - 7.54 (m, 3 H) 7.59 (t, *J*=7.42 Hz, 1 H) 7.70 (t, *J*=7.22 Hz, 1 H) 7.76 (d, *J*=7.42 Hz, 1 H) 8.13 (s, 1 H). ^{13}C NMR (101 MHz, DMSO-d6) δ ppm 113.41, 114.86, 119.08, 119.83, 124.63, 125.24, 125.49, 126.86, 129.00, 132.53, 134.67, 144.21, 146.97, 147.47, 156.51, 157.99, 159.60. FT-IR (cm^{-1}) 688, 730, 749, 813, 860, 910, 927, 998, 1042, 1089, 1157, 1217, 1259, 1277, 1307, 1328, 1382, 1448, 1458, 1489, 1509, 1571, 1578, 1615, 2937, 3063, 3277. ESI–MS (m/z): 403.1.

*Data for **2***

^{1}H NMR (400 MHz, $CDCl_3$) δ ppm 2.24 (s, 3 H) 2.29 (s, 3 H) 6.70 (s, 1 H) 6.94 (t, *J*=7.62 Hz, 1 H) 7.01 (d, *J*=8.20 Hz, 1 H) 7.08 (t, *J*=7.62 Hz, 1 H) 7.19 - 7.31 (m, 3 H) 7.33 - 7.53 (m, 4 H) 7.65 (d, *J*=8.20 Hz, 2 H) 8.06 (s, 1 H) 8.16 (d, *J*=8.2 Hz, 1 H). ^{13}C NMR (101 MHz, DMSO-d_6) δ ppm 19.57, 20.48, 117.03, 117.50, 119.38, 120.10, 120.90, 121.99, 126.95, 127.60, 128.71, 129.23, 129.53, 133.15, 135.62, 136.45, 138.75, 140.68, 143.23, 154.41, 156.63, 160.13, 163.70. FT-IR (cm^{-1}) 687, 721, 753, 799, 863, 901, 919, 1021, 1048, 1071, 1127, 1157, 1210, 1230, 1262, 1292, 1311, 1328, 1373, 1384, 1447, 1474, 1490, 1506, 1553, 1575, 1619, 2922, 2964, 3062, 3241. ESI–MS (m/z): 431.1.

*Data for **3***

^{1}H NMR (400 MHz, $CDCl_3$) δ ppm 6.56 (s, 1 H), 6.85 (s, 1 H), 7.48 - 7.66 (m, 4 H), 7.66 - 7.82 (m, 3 H), 7.86 - 8.17 (m, 5 H). FT-IR (cm^{-1}) 684, 701, 723, 754, 799, 842, 863, 880, 912, 1019, 1084, 1163, 1260, 1351, 1376, 1449, 1481, 1583, 1617, 2963, 3066, 3100. ESI–MS (m/z): 468.0.

*Data for **4***

^{1}H NMR (400 MHz, $CDCl_3$) δ ppm 7.06 (t, *J*=7.56 Hz, 1 H), 7.26 - 7.34 (m, 2 H), 7.42 - 7.64 (m, 7 H), 7.71 (t, *J*=8.01 Hz, 1 H), 7.90 (d, *J*=8.24 Hz, 1 H), 8.11 (d, *J*=8.24 Hz, 1 H), 8.19 (d, *J*=8.24 Hz, 2 H), 9.25 (br. s., 1 H). ^{13}C NMR (101 MHz, $CDCl_3$) δ ppm 113.97, 115.52, 120.48, 121.23, 122.06, 124.85, 125.01, 125.72, 127.81, 128.72, 129.61, 129.75, 130.46, 132.61, 138.37, 140.88, 144.18, 146.48, 154.91, 158.36. FT-IR (cm^{-1}) 656, 690, 718, 745, 759, 771, 819, 856, 895, 949, 983, 999, 1017, 1032, 1059, 1090, 1124, 1155, 1164,1200, 1218, 1247, 1259, 1294, 1311, 1318, 1342, 1384, 1416, 1446, 1457, 1478, 1523, 1548, 1584, 1607, 1624, 2928, 3066, 3099. ESI–MS (*m/z*): 453.05.

*Data for **5***

^{1}H NMR (400 MHz, DMSO-d_6) δ ppm 2.25 (d, *J*=7.02 Hz, 6 H), 7.30 (s, 1 H), 7.47 - 7.66 (m, 5 H), 7.79 (t, *J*=7.67 Hz, 1 H), 7.98 (s, 1 H), 8.00 - 8.11 (m, 3 H), 8.39 (d, *J*=8.77 Hz, 1 H), 8.56 (d, *J*=8.77 Hz, 1 H), 10.04 (s, 1 H). ^{13}C NMR (101 MHz, DMSO-d_6) δ ppm 19.2, 20.3, 111.6, 115.3, 117.2, 120.3, 122.2, 125.5, 127.7, 128.1, 129.1, 129.2, 130.9, 131.4, 132.9, 135.2, 139.2, 140.0, 140.2, 150.0, 157.5. FT-IR (cm^{-1}) 689, 716, 740, 749, 768, 805, 833, 848, 865, 870, 875, 894, 950, 976, 1038, 1049, 1089, 1116, 1145, 1162, 1203, 1219, 1277, 1295, 1312, 1333, 1374, 1390, 1415, 1448, 1456, 1488, 1524, 1546, 1581, 1604, 1622, 2860, 2915, 2935, 2971, 3008, 3060, 3081. ESI–MS (m/z): 481.2.

*Data for **6***

^{1}H NMR (400 MHz, $CDCl_3$) δ ppm 6.55 (s, 1H), 6.85 (s, 1H), 6.91 – 6.98 (m, 1H), 7.07 – 7.17 (m, 2H), 7.55 – 7.59 (m, 2H), 7.69 – 7.82 (m, 2H), 7.97 – 8.28 (m, 8H). FT-IR (cm^{-1}) 681, 703, 721, 738, 752, 817, 848, 863, 880, 913, 982, 1000, 1024, 1083, 1131, 1166, 1253, 1278, 1313, 1357, 1377, 1449, 1466, 1484, 1561, 1584, 1598, 1624, 2921, 2964, 3063, 3098. ESI–MS (*m/z*): 523.1.

Computational procedure

Model construction and visualization were conducted utilizing GaussView 5 [28], whereas all quantum-chemical computations were executed with the Gaussian 09 software suite [28]. Ground-state geometries were optimized employing the HSEH1PBE density functional [28] in conjunction with the cc-pVDZ basis set [28]. Electronic excitations and the simulated UV-Vis absorption spectrum were derived using time-dependent DFT (TD-DFT) method [28] at the same level. The integral equation formalism of the polarizable continuum model (IEF-PCM) [28] was employed to incorporate solvent effects. Orbital composition analysis, encompassing the fractional contributions of fragments to molecular orbitals and the identification of primary configurations influencing TD-DFT transitions were conducted utilizing GaussSum software [28].

3. Results and Discussions

Synthesis and Characterization

In this study, **La-c** compounds were synthesized by reacting 1,2-diaminobenzene derivatives with benzene sulfonyl chloride in dichloromethane (DCM) in the presence of triethylamine (TEA). **L(1,2)(a-c)** ligands were synthesized by reacting **La-c** compounds with salicylaldehyde and 2-hydroxy naphthaldehyde, respectively. The reaction of **L1-2**

compounds with $BF_3.OEt_2$ in toluene, in the presence of TEA, obtained new Schiff base-borane complexes (**1-6**). The structures of the synthesized compounds were characterized using NMR, FTIR, and MS techniques. The synthesis steps of the compounds are illustrated in Fig. 1.

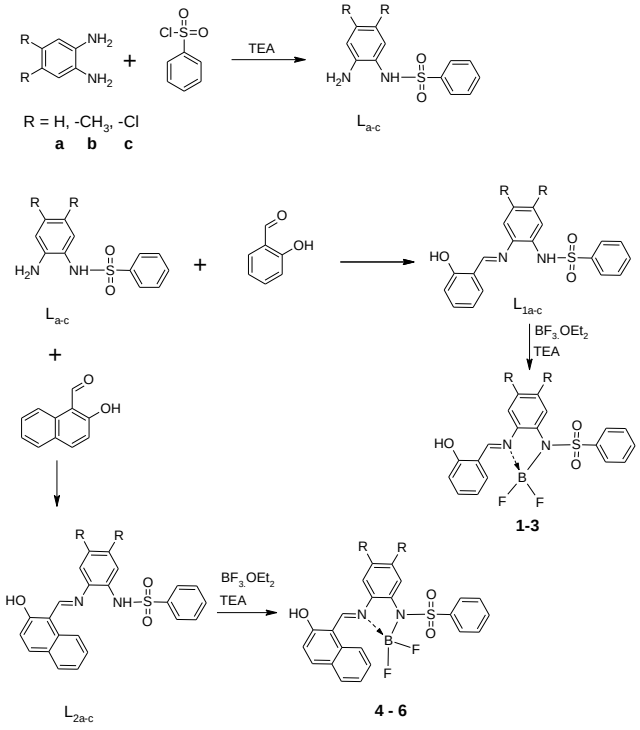

Figure 1. Synthesis of compounds

When the ^{1}H-NMR spectra of **L1b-c** were analyzed, the -C*H*=N- protons were observed as single peaks at 8.05 ppm and 8.54 ppm, respectively, while the -O*H* protons appeared as single peaks at 11.89 ppm and 12.56 ppm, respectively. In the ^{13}C-NMR spectra of **L1b-c**, the -*C*H=N- carbons were located at 160.35 and 161.32 ppm, respectively, while the -*C*-O carbons were found at 163.96 and 164.63 ppm, respectively. The -*C*H_3 carbons of L2b were observed at 19.42 and 19.55 ppm. The obtained values are in good agreement with reported literature data [22].

When the ^{1}H-NMR spectra of **L2a-c** were analyzed, the -C*H*=N- protons were observed as singlets at 8.93 ppm, 8.84 ppm, and 10.84 ppm, respectively. The -C*H*$_3$ protons of **L2b** appeared as singlets at 2.28 ppm and 2.32 ppm. Signals corresponding to other aromatic protons were observed as multiple peaks within the 7.00-9.00 ppm range. In the ^{13}C-NMR spectra of **L2a-c**, the -*C*H=N- carbons were detected at 161.0 ppm, 159.42 ppm, and 157.8 ppm, respectively, while the -**C**-O carbons appeared at 163.3 ppm, 164.0 ppm, and 165.0 ppm, respectively. The -*C*H_3 carbons of **L2b** were observed as singlets at 19.5 ppm and 19.6 ppm. The obtained values are in good agreement with reported literature data [27].

When analyzing the ^{1}H-NMR spectra of compounds **1** and **2** derived from **L1a-b**, the -C*H*=N- protons appeared as singlets at 8.13 and 8.16 ppm, respectively. In compound **3** derived from **L1c**, the -C*H*=N- protons were observed as multiple peaks within the 7.86 - 8.17 ppm range. The -C*H*$_3$ protons of compound **2** were detected as singlets at 2.24 ppm and 2.29 ppm. Generally, the ^{13}C-NMR spectra of the synthesized compounds are consistent with their proposed structures. However, the ^{13}C-NMR spectra of compounds **3** and **6** could not be recorded due to their poor solubility.

When analyzing the ^{1}H-NMR spectra of compounds **4** and **5** derived from **L2a-b**, the -C*H*=N- protons appeared as singlets at 9.25 ppm and 10.04 ppm, respectively. In contrast, the -C*H*=N- protons of compound **6** derived from **L2c** were observed within the 7.97-8.28 ppm range. The -C*H*$_3$ protons of compound **5** appeared as a doublet at 2.25 ppm. In the ^{13}C-NMR spectrum of **5**, the -CH_3 carbons were detected at 19.2 ppm and 20.3 ppm.

In the FT-IR spectrum of **L1b-c**, N-H stretching vibrations were observed at 3354 cm^{-1} and 3377 cm^{-1}, while -C=N- stretching vibrations appeared at 1617 cm^{-1} and 1620 cm^{-1}. Additionally, the asymmetric S=O stretching vibrations of **L1b-c** were detected at 1328 cm^{-1} and 1314 cm^{-1}, respectively.

In the FT-IR spectra of **L2a-c**, N-H stretching vibrations were observed at 3246 cm^{-1} for **L2a** and 3410 cm^{-1} for **L2c**, while no N-H stretching was detected for **L2b**. Additionally, N-H bending vibrations appeared at 1592 cm^{-1}, 1602 cm^{-1}, and 1588 cm^{-1} for **L2a-c**, respectively.

In the FT-IR spectrum, the C=N stretching vibrations were observed at 1618 cm^{-1} for **L2a**, 1617 cm^{-1} for **L2b**, and 1620 cm-1 for **L2c**. The asymmetric and symmetric stretching vibrations of the S=O_2 group appeared at 1320 cm^{-1} and 1163 cm^{-1} for L2a, 1352 cm^{-1} and 1156 cm^{-1} for **L2b**, and 1313 and 1175 cm^{-1} for **L2c**, respectively. These results are consistent with previously reported literature [27].

In complexes **1-3**, formed through the complexation of **L1a-c** compounds, the C=N stretching vibrations were observed at 1615 cm^{-1}, 1619 cm^{-1}, and 1617 cm^{-1}, respectively. The asymmetric and symmetric stretching vibrations of the S=O2 group were identified at 1328 cm^{-1} and 1157 cm^{-1} for complexes **1** and **2** and at 1351 cm^{-1} and 1163 cm^{-1} for complex **3**, respectively.

In complexes **4-6**, formed through the complexation of **L2a-c** compounds, the C=N stretching vibrations were observed at 1624 cm^{-1}, 1622 cm^{-1}, and 1624 cm^{-1}, respectively. The asymmetric and symmetric stretching vibrations of the S=O_2 group appeared at 1318 cm^{-1} and 1155 cm^{-1} for complex **4**, at 1312 cm^{-1} and 1145 cm^{-1} for complex **5**, and at 1357 cm^{-1} and 1166 cm^{-1} for complex **6**, respectively.

Optical properties

The UV-Vis spectra of the compounds are presented in Figure 2. The $\pi \rightarrow \pi^*$ transition peaks for compounds **L1a-c**

were observed at 410, 416, and 367 nm, respectively. Upon complexation, the π→π* transition peaks for complexes **1-3** appeared at 416, 414, and 440 nm, respectively. The bathochromic shift associated with increased conjugation is clearly evident for compounds **L2a-c**, with n→π* transitions peaks observed at 440, 440, and 385 nm, respectively. Under the complexation of **L2a-c**, the n→π* transition peaks for complexes **4-6** were observed at 438, 443, and 390 nm, respectively.

The optical band gaps of compounds **1-6** were determined from their UV-Vis spectra using the method reported in the literature [29]. While the theoretical calculations successfully predict the trend in electronic properties of the complexes, a notable discrepancy of approximately 1.3 eV was observed between the experimental and theoretical optical band gaps (Table 1). The experimental values are significantly lower than the calculated ones. This difference is attributed to the fact that standard gas-phase DFT calculations do not account for intermolecular interactions (e.g. π-π stacking or aggregations). Therefore, the theoretical results should be viewed as a qualitative guide for the electronic structure rather than exact quantitative predictions.

Table 1. UV-visible spectral characteristics of $1.25x10^{-5}$ M methanolic solutions of the synthesized complexes.

Compound	λ/nm (Σ/$M^{-1}.cm^{-1}$)	E_{bb} (eV)	$E_{bb\text{-}teo}$ (eV)
1	416 (2976), 328 (12992), 292 (14936)	2.58	3.92
2	414 (7208), 300 (11112)	2.45	3.74
3	440 (576), 324 (7752), 310 (7832)	2.51	3.81
4	438 (2984), 327 (4592), 305 (5680)	2.42	3.28
5	443 (1168), 323 (2216), 304 (3456)	2.37	3.30
6	390 (2504), 373 (2808), 319 (8808)	2.29	3.22

λ: Maximum absorption wavelength

Σ: Molar absorption coefficient

E_{bb}: Band gap

$E_{bb\text{-}teo}$: Theoretical band gap

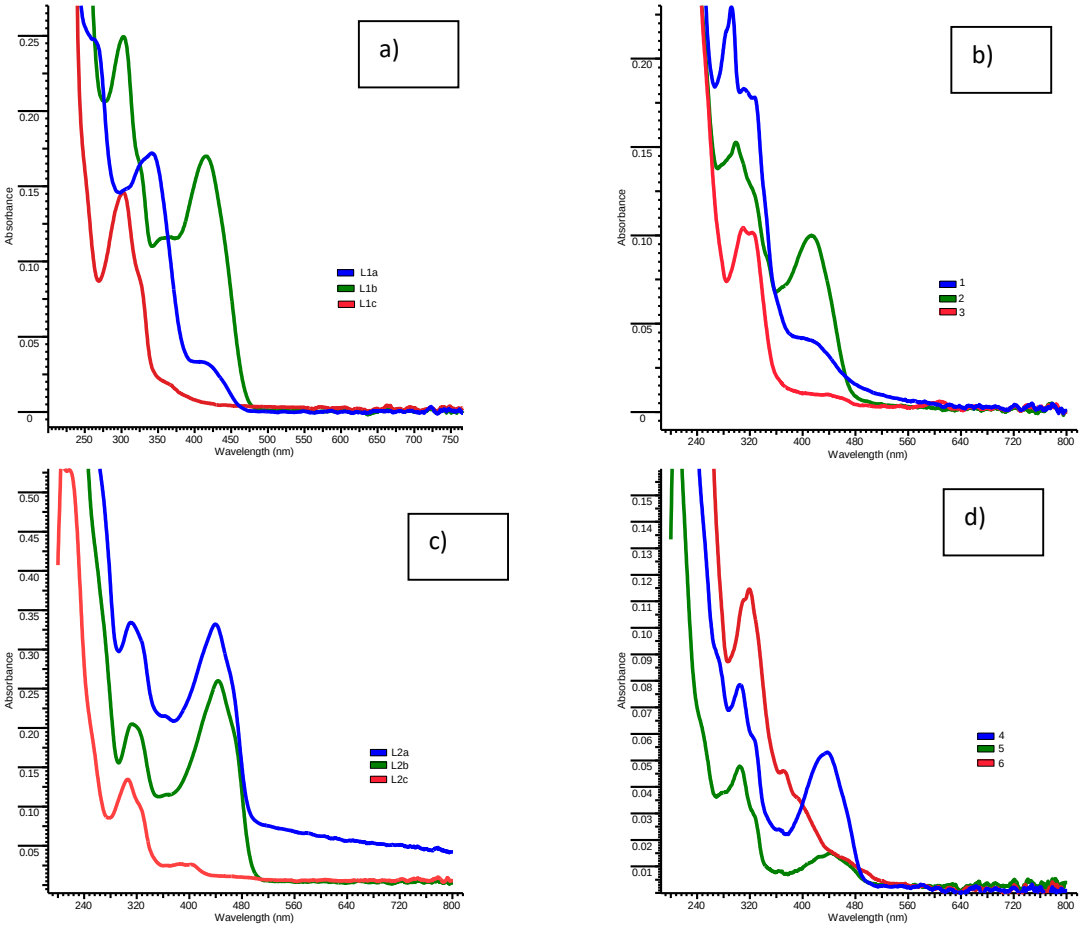

Figure 2. UV-Vis spectra of 1.25×10^{-5} M a) **L1a–c**, b) **1–3**, c) **L2a–c**, d) **4–6** in methanol

	1	2	3	4	5	6
LUMO+1	-1.72 eV	-1.64 eV	-1.92 ev	-1.74 eV	-1.65 eV	-1.93 eV
LUMO	-3.02 eV	-2.93 eV	-3.24 eV	-3.18 eV	-3.11 eV	-3.39 eV
HOMO	-6.94 eV	-6.67 eV	-7.05 eV	-6.46 eV	-6.41 eV	-6.61 eV
HOMO-1	-7.08 eV	-6.99 eV	-7.26 eV	-6.94 eV	-6.67 eV	-7.03 eV

Figure 3. Isodensity surface plots of HOMOs and LUMOs with energy levels for **1-6** complexes.

The optical properties of the synthesized Schiff base ligands (**L1a-c** and **L2a-c**) and their corresponding boron complexes (**1-6**) were investigated in methanol solution under both sunlight and UV light (375 nm) (Fig. 4). The ligands (**L1-2**) exhibited a transparent appearance ranging from pale yellow to dark yellow under sunlight (Fig. 4a), whereas they displayed no notable fluorescence emission or only very weak emission under 375 nm UV illumination (Fig. 4b). In contrast, the boron complexes (**1-6**), formed by incorporating boron difluoride groups into the molecular structure, induced significant changes in photophysical properties. These complexes, which appeared in yellow-orange tones similar to the ligands under sunlight (Fig. 4c), exhibited strong and bright fluorescence visible to the naked eye under UV excitation (Fig. 4d). It was observed that derivatives containing a naphthalene ring, in particular, exhibited broader emission color variations spanning from blue to orange.

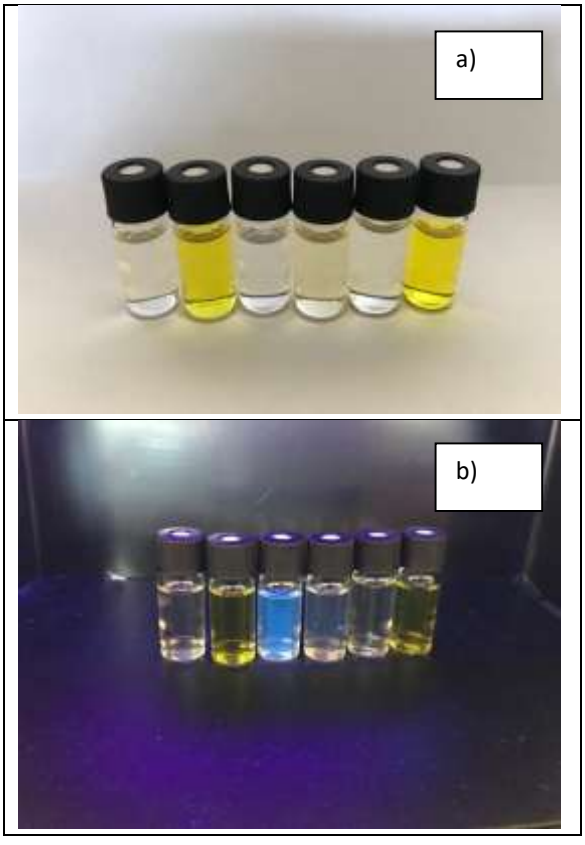

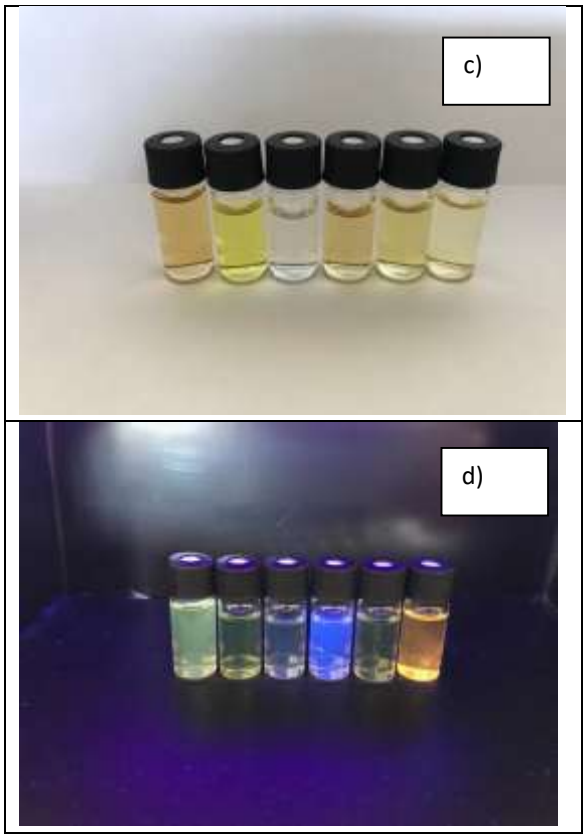

Figure 4. a) Appearance of ligands under sunlight (from left to right: L1a, L2a, L1b, L2b, L1c, L2c); b) Appearance of ligands under 375 nm light (from let to right: L1a, L2a, L1b, L2b, L1c, L2c); c) Appearance of boron complexes under sunlight (from left to right: 1, 4, 2, 5, 3, 6); d) Appearance of boron complexes under 375 nm light (from let to right: 1, 4, 2, 5, 3, 6)

4. Conclusion

In this paper, three monosulphonated 1,2-diamine derivatives (**La-c**) were synthesized from reactions between three 4,5-disubstituted-1,2-diaminobenzene derivatives and benzenesulfonyl chloride in the presence of triethylamine. Subsequent Schiff base reactions of La-c derivatives with 2-hydroxyaldehyde derivatives in ethanol yielded six 2-hydroxyaldimine derivatives (**L1a-c** and **L2a-c**) containing a sulfonamide group. New boron complexes were then obtained by reacting these ligands (**L1a-c** and **L2a-c**) with $BF_3.OEt_2$ in the presence of triethylamine in toluene. All compounds were characterized using NMR, IR, and ESI-MS techniques. The optical properties of the synthesized compounds were also examined. It was observed that UV-Vis spectra of the ligands and their corresponding boron complexes are quite similar, and that the spectra of the boron complexes consist mainly of three bands. The optical band gap values derived from the UV-Vis spectra were approximately 2.5 eV, while the theoretically calculated band gap values range between 3.22 and 3.92 eV. The discrepancy between the theoretical and experimental results is believed to arise from interactions between the

synthesized molecules and the solvent. Most of the synthesized molecules display fluorescence under 375 nm light in methanol. The distinct variations in fluorescence color caused by slight modifications in the compound skeleton are noteworthy. In conclusion, it was determined that the boron complexes prepared with simple Schiff bases exhibit photoluminescence properties and that minor changes in the molecular skeleton directly influence the photoluminescence color.

Acknowledgements

This research has been supported by Çanakkale Onsekiz Mart University Scientific Research Projects Commission (Project No: FBA-2018-1364).

References

[1] K. Dhanunjayarao, V. Mukundam, R.V.R.N. Chinta, K. Venkatasubbaiah, Synthesis of highly fluorescent imidazole based diboron complex, J Organomet Chem 865 (2018) 234-238.

[2] A. Loudet, K. Burgess, BODIPY dyes and their derivatives: Syntheses and spectroscopic properties, Chem Rev 107(11) (2007) 4891-4932.

[3] G. Ulrich, R. Ziessel, A. Harriman, The chemistry of fluorescent bodipy dyes: Versatility unsurpassed, Angewandte Chemie-International Edition 47(7) (2008) 1184-1201.

[4] N. Boens, V. Leen, W. Dehaen, Fluorescent indicators based on BODIPY, Chem Soc Rev 41(3) (2012) 1130-1172.

[5] A. Kamkaew, S.H. Lim, H.B. Lee, L.V. Kiew, L.Y. Chung, K. Burgess, BODIPY dyes in photodynamic therapy, Chem Soc Rev 42(1) (2013) 77-88.

[6] T. Yogo, Y. Urano, Y. Ishitsuka, F. Maniwa, T. Nagano, Highly efficient and photostable photosensitizer based on BODIPY chromophore, J Am Chem Soc 127(35) (2005) 12162-12163.

[7] S.H. Lo, M.C. Wu, S.P. Wu, A turn-on fluorescent sensor for cysteine based on BODIPY functionalized Au nanoparticles and its application in living cell imaging, Sensor Actuat B-Chem 221 (2015) 1366-1371.

[8] L. Bonardi, H. Kanaan, F. Camerel, P. Jolinat, P. Retailleau, R. Ziessel, Fine-tuning of yellow or red photo- and electroluminescence of functional difluoro-boradiazaindacene films, Adv Funct Mater 18(3) (2008) 401-413.

[9] D. Frath, S. Azizi, G. Ulrich, P. Retailleau, R. Ziessel, Facile Synthesis of Highly Fluorescent Boranil Complexes, Org Lett 13(13) (2011) 3414-3417.

[10] J. Massue, D. Frath, G. Ulrich, P. Retailleau, R. Ziessel, Synthesis of Luminescent 2-(2 '-Hydroxyphenyl)benzoxazole (HBO) Borate Complexes, Org Lett 14(1) (2012) 230-233.

[11] D. Frath, A. Poirel, G. Ulrich, A. De Nicola, R. Ziessel, Fluorescent boron(III) iminocoumarins (Boricos), Chem Commun 49(43) (2013) 4908-4910.

[12] S. Chibani, A. Charaf-Eddin, B. Le Guennic, D. Jacquemin, Boranil and Related NBO Dyes: Insights From Theory, J Chem Theory Comput 9(7) (2013) 3127-3135.

[13] J. Shanmugapriya, K. Rajaguru, G. Sivaraman, S. Muthusubramanian, N. Bhuvanesh, Boranil dye based "turn-on" fluorescent probes for detection of hydrogen peroxide and their cell imaging application, Rsc Adv 6(89) (2016) 85838-85843.

[14] S. Deshpande, H. Kumbhar, G. Shankarling, Photoswitchable conjugated assembly involving fluorescent boranil, J Lumin 179 (2016) 314-321.

[15] M. Urban, K. Durka, P. Jankowski, J. Serwatowski, S. Lulinski, Highly Fluorescent Red-Light Emitting Bis(boranils) Based on Naphthalene Backbone, J Org Chem 82(15) (2017) 8234-8241.

[16] W.Q. Chen, L.L. Zhu, Y.Q. Hao, X.X. Yue, J.Y. Gai, Q. Xiao, S. Huang, J.R. Sheng, X.Z. Song, Detection of thiophenol in buffer, in serum, on filter paper strip, and in living cells using a red-emitting amino phenothiazine boranil based fluorescent probe with a large Stokes shift, Tetrahedron 73(31) (2017) 4529-4537.

[17] A. Iwan, D. Sek, Processible polyazomethines and polyketanils: From aerospace to light-emitting diodes and other advanced applications, Prog Polym Sci 33(3) (2008) 289-345.

[18] H.P. Liu, Z.Q. Lu, Z.L. Zhang, Y. Wang, H.Y. Zhang, Highly Elastic Organic Crystals for Flexible Optical Waveguides, Angew Chem Int Edit 57(28) (2018) 8448-8452.

[19] J. Zhang, L.L. Xu, W.Y. Wong, Energy materials based on metal Schiff base complexes, Coordin Chem Rev 355 (2018) 180-198.

[20] A. Majumder, G.M. Rosair, A. Mallick, N. Chattopadhyay, S. Mitra, Synthesis, structures and fluorescence of nickel, zinc and cadmium complexes with the N,N,O-tridentate Schiff base N-2-pyridylmethylidene-2-hydroxy-phenylamine, Polyhedron 25(8) (2006) 1753-1762.

[21] N. Aksuner, E. Henden, I. Yilmaz, A. Cukurovali, A highly sensitive and selective fluorescent sensor for the determination of copper(II) based on a schiff base, Dyes Pigments 83(2) (2009) 211-217.

[22] N. Özdemir, S. Dayan, O. Dayan, M. Dinçer, N.Ö. Kalaycıoğlu, Experimental and molecular modeling investigation of (E)-N-{2-[(2-hydroxybenzylidene)amino]phenyl}benzenesulfonamide, Mol Phys 111(6) (2013) 707-723.

[23] S. Dayan, F. Arslan, N. Kalaycioglu Ozpozan, Ru(II) impregnated Al2O3, Fe3O4, SiO2 and N-coordinate ruthenium(II) arene complexes: Multifunctional catalysts in the hydrogenation of nitroarenes and the transfer hydrogenation of aryl ketones, Applied Catalysis B: Environmental 164 (2015) 305-315.

[24] N. Kayaci, S. Dayan, N. Kalaycioglu Ozpozan, Novel N-coordinate half-sandwich ruthenium(II) arene complexes bearing sulfonamide fragments: Catalytic activities in the TH of acetophenone derivatives, J Mol Struct 1099 (2015) 446-452.

[25] Z. Demircioğlu, F.A. Özdemir, O. Dayan, Z. Şerbetçi, N. Özdemir, Synthesis, X-ray diffraction method, spectroscopic characterization (FT-IR, 1H and 13C NMR), antimicrobial activity, Hirshfeld surface analysis and DFT computations of novel sulfonamide derivatives, J Mol Struct 1161 (2018) 122-137.

[26] J.H. Billman, R.L. Schmidgall, Preparation and Antitumor Activity of Some Schiff Bases of 2′-Amino-4′, 5′-Dichlorobenzenesulfonanilide and 2′-Amino-p-Toluenesulfonanilide, Journal of Pharmaceutical Sciences 59(8) (1970) 1191-1194.
[27] M. Tercan, N. Özdemir, F.A. Özdemir, Z. Şerbetçi, D. Erdener, B. Çetinkaya, O. Dayan, Synthesis, DFT computations and antimicrobial activity of a Schiff base derived from 2-hydroxynaphthaldehyde: Remarkable solvent effect, Journal of Molecular Structure 1209 (2020) 127980.
[28] S. Bruker, S. SAINT, Bruker AXS Inc, Madison, Wisconsin, USA (2002).
[29] K. Colladet, M. Nicolas, L. Goris, L. Lutsen, D. Vanderzande, Low-band gap polymers for photovoltaic applications, Thin Solid Films 451–452 (2004) 7-11.